

Role of PET/CT in lung cancer

Essay

Submitted for partial fulfillment of Master
degree in Radiodiagnosis

By:

Mohamed Ghareeb Abdrabo Abozeid

M.B., B.C H.

Cairo University

Under supervision of:

Prof. Dr. / Sahar Farouk Shaaban

Professor of radiodiagnosis

Faculty of medicine

Ain shams university

Dr. / Ahmed Samir Ibrahim

Lecturer of radiodiagnosis

Faculty of medicine

Ain shams university

2009

Acknowledgement

*First and foremost my deep thanks to **ALLAH**.*

*It is a pleasure to express sincere appreciation and deepest gratitude to **Dr. Sahar Farouk Shaban**, Professor of Radiodiagnosis, Faculty of Medicine, Ain Shams University, for her greatest support, continuous guidance and encouragement through this whole work,*

*I deeply thank **Dr. Ahmed Samir Ibrahim**, Lecturer of Radiodiagnosis, Faculty of Medicine, Ain Shams University, for his kind guidance, helpful suggestion and valuable advice.*

Mohamed Ghareeb.

List of Abbreviations

FDG	= F-18FDG=18F-fluorodeoxyglucose = Fluorine- F-18 Fluoro-2-deoxy-D-glucose
ACF	=Attenuation Correction Factor
AJCC	=American Joint Commission for Cancer
BGO	=Bismuth Germinate
CE-CT	=Contrast Enhanced CT
CT	=Computed Tomography
DNA	=Deoxyribonucleic Acid
FOV	=Field Of View
GLUT	=Glucose Transporters
H+	=Hydrogen ions
HU	=Hounsfield Units
I.V	=Intravenous
keV	=kilo electron volt
LL	=Lower Lobe
LBG	=Locust Bean Gum
LSO	=Lutetium Oxyorthosilicate
mA	=milliampere
MAS	= Milli Ampere Second
MBq	=mega becquerel
mCi	=millicurie
MeV	=Mega electron Volt
MRI	=Magnetic Resonance Imaging
NSCLC	= Non Small Cell Lung Cancer

PET	=Positron Emission Tomography
PET/CT	=Positron Emission Tomography/ Computed Tomography
PMTs	=Photomultiplier Tubes
PPV	=Positive Predictive Value
R&L	=Right and left
RLL	=Right Lower Lobe
RML	=Right Middle Lobe
SCLC	= Small Cell Lung Cancer
SPECT	=Single Photon Emission Computed CT
SUVs	=Standard Uptake Values
TNM	=Tumor, Node, Metastasis
WHO	=World Health Organization
¹³N	=Nitrogen-13
¹¹C	=Carbon-11
¹⁸O	=Oxygen-18
¹¹C-CHO	= ¹¹ C-Cholin
¹³NH₃	= ¹³ N-ammonia
β⁻	=electrons
β⁺	=Positrons

List of Figures

Fig. No.		Page No.
Fig. (1)	Normal distribution of FDG. Coronal CT (a), PET (b), and PET/CT fusion (c).....	7
Fig. (2)	PET/CT image consisting of coronal whole-body CT image (A), PET image with CT attenuation correction (B), and fused image (C).....	8
Fig. (3)	Normal FDG-PET whole-body scan.....	12
Fig. (4)	Bronchopulmonary segments in CT scan	14
Fig. (5)	Regional lymph node stations for lung cancer staging	15
Fig. (6)	CT anatomy: level T2	18
Fig. (7)	CT anatomy: level T3,4	18
Fig. (8)	CT anatomy: level T4,5	19
Fig. (9)	CT anatomy: level T5	19
Fig. (10)	CT anatomy: level T6	20
Fig. (11)	CT anatomy: level T8,9	20
Fig. (12)	Early metabolic paths of glucose and FDG	44
Fig. (13)	Annihilation reaction	45
Fig. (14)	Typical scout image obtained during an FDG PET/CT study	53
Fig. (15)	Current commercial PET/CT scanners from 3 vendors	56
Fig. (16)	Complete PET/CT image display of a 65-year-old patient with lung cancer on the left side and a brain metastasis.....	58
Fig. (17)	Display screen of software platform shows fused PET/CT images in the sagittal, coronal, and axial planes of a patient with recurrent esophageal carcinoma.....	59
Fig. (18)	Attenuation correction artifact.....	68

List of Figures (Cont...)

Fig. No.		Page No.
Fig. (19)	Attenuation correction artifact.....	68
Fig. (20)	Large cell lung carcinoma in a 64-year-old man	69
Fig. (21)	Solitary pulmonary nodule with spiculated borders in left upper lobe.....	71
Fig. (22)	Metabolically active pulmonary nodule and the histological diagnosis was NSCLC	74
Fig. (23)	Solitary pulmonary nodule. Benign or malignant?.....	75
Fig.(24a,b,c)	A 52-year-old woman with a newly diagnosed lung adenocarcinoma.....	83
Fig. (25a,b)	A 57-year-old woman with newly diagnosed, poorly differentiated lung adenocarcinoma	84
Fig.(26a,b,c,d)	A 62-year-old woman with adenocarcinoma of the right lower lobe.....	87
Fig. (27a,b,c)	A 52-year-old man with a newly diagnosed Pancoast tumor of the right superior sulcus and palpable right supraclavicular lymphadenopathy.....	91
Fig.(28a,b,c,d,e,f)	A 52-year-old woman with NSCLC of the right upper lobe and known pneumonia	93
Fig. (29a,b,c)	A 75-year-old man with newly diagnosed lung adenocarcinoma	96
Fig. (30a,b,c)	CT, PET and PET/CT in a patient with lung cancer of right upper lung lobe.....	103
Fig. (31a,b,c)	CT, PET and PET/CT in a patient with lung cancer of left lower lung lobe with no nodal involvement	104
Fig. (32a,b,c)	CT, PET and PET/CT in a patient with lung cancer of right upper lung lobe with lymph node metastasis	105

List of Figures (Cont...)

Fig. No.		Page No.
Fig. (33a,b,c)	CT, PET and PET/CT in a patient with pubic bone metastasis	106
Fig.(34a,b,c)	CT, PET and PET/CT in a patient with lung cancer of right middle lung lobe with right upper lobe metastasis	107
Fig.(35a,b,c,d)	A 51-year-old woman with total collapse of the left upper lobe of her lung secondary to a large adenocarcinoma at the left hilum (stage III NSCLC).	110
Fig. (36a,b,c,d)	A 72-year-old man with a known poorly differentiated NSCLC of the right lung apex.....	113
Fig. (37)	Recurrence adjacent to radiation therapy field.....	118

List of Tables

Tab. No.		Page No.
Table (1)	Lung segments	13
Table (2)	Lymph Node Map Definitions (Nodal Stations).....	16,17
Table (3)	Signs and symptoms of pulmonary carcinoma: pathologic correlation.....	26
Table (4)	Signs and symptoms of bronchogenic carcinoma.....	27
Table (5)	histologic classification of primary lung tumors.....	28
Table (6)	TNM Classification (International Staging System of Lung Cancer)	40
Table (7)	Stage grouping TNM subsets	41
Table (8)	Radionuclides Used in PET.....	46
Table (9)	The (TNM) staging system	77,78,79
Table (10)	International Staging System for NSCLC, Including Stage Groups and TNM Subsets.....	79

AIM OF THE WORK

To evaluate the role of fused PET-CT images in diagnosis, staging and follow up of patients with lung cancer hoping to reach an effective treatment.

Introduction

Cancer is one of the leading causes of morbidity and mortality even in developed countries. Complex clinical decisions about treatment of tumors are largely guided by imaging findings, among other factors. Most radiological procedures map the anatomy and morphology of tumors with little or no information about their metabolism (*Kapoor et al., 2004*).

In the past 2 decades, computed tomography (CT) has been the main diagnostic tool in initial staging of disease and therapy follow-up in patients with cancer. Morphologic changes depicted at CT have been equated to disease manifestations. CT has proved to be an accurate imaging modality for various cancers and has been used in the treatment decision making process (*Hany et al., 2002*).

Advances in surgical techniques and radiotherapy, together with an explosion in drug trials, have driven exciting developments in imaging. Improvements in hardware technology and image processing allow the routine acquisition of high-quality multiplanar images of the body through the use of computed tomography (CT) and magnetic resonance imaging (MRI). Such imaging is increasingly used to provide detailed road maps for planning surgery and radiotherapy. In addition, clinical trials are placing a greater reliance on imaging to provide noninvasive, objective measures of the response of the tumor to therapy. The use of

Introduction

functional imaging techniques will enable us to assess changes in tumor biology during and after treatment. The diagnostic and prognostic importance of imaging-derived estimates of tumor perfusion, permeability, blood volume, and hypoxia is being widely evaluated. The fusion of two imaging techniques, such as positron-emission tomography (PET) and CT, offers the potential of combining anatomical with functional information (*Lardinois et al., 2003*).

In certain situations, it may be impossible to accurately localize an area of increased activity on PET images alone due to the absence of identifiable anatomic structures, particularly in the abdomen. Investigators recognized this limitation in oncology imaging, and therefore attempts at developing algorithms to co register functional and anatomic information have had varying success in the past decade (*Beyer et al., 2000*).

Accurate evaluation of disease extent prior to therapy and of response to therapy have a significant impact on the clinical management of oncologic disorders. Co-registration of PET scans (functional and morphologic information) with computed tomographic (CT) scans (anatomic information) using a combined PET/CT scanner improves the overall sensitivity and specificity of information provided by PET or CT alone. The unique advantage of PET/CT fusion imaging is the ability to correlate findings at two complementary imaging modalities in a comprehensive examination. Hence, PET/CT provides more precise anatomic

Introduction

definition for both the physiologic and pathologic uptake seen at FDG PET (*Goerres et al., 2002*).

Physiologic FDG uptake in nonmalignant conditions limits the specificity of PET, particularly in the post therapy setting. Hybrid PET/CT scanners allow PET and CT image fusion for differentiation of physiologic variants from juxtaposed or mimetic neoplastic lesions and more accurate tumor localization. Software based fusion of separately acquired PET and CT scans is more likely to lead to mis-registration due to independent parameters and differences in patient positioning (*Bar-Shalom et al., 2003*).

Described the prototype PET/CT scanner used in clinical imaging, in which precisely co registered functional and anatomic images could be obtained by performing a PET study and a CT study on the same scanner without moving the patient. Although the limit of resolution of PET alone as compared with that of PET/CT remains the same, the overall combination aids in the accurate localization of regions of increased activity on PET images with greater confidence.

In particular, in the post therapy period, subtle metabolic findings at FDG PET that might otherwise be overlooked may allow detection of residual disease after correlation with the simultaneously acquired CT data. Conversely, equivocal CT findings can be better evaluated with the help of the additional functional information provided by FDG PET (*Kostakoglu et al., 2004*).

Introduction

In tumor imaging PET/CT has become the clinicians' scanning procedure of choice in a short time. Owing to its faster acquisition time compared with a “conventional” dedicated PET scanner, PET/CT improves patient comfort and decreases patient examination time (*Steinert and Von Schulthess, 2002*).

Use of dual-modality PET/CT significantly increases the number of patients with correctly staged non-small cell lung cancer (NSCLC) and thus has a positive effect on treatment (*Antoch et al., 2003*).

The most important prognostic indicator in lung cancer is the extent of disease. The Union Internationale Contre le Cancer (UICC) and the American Joint Committee for Cancer Staging (AJCC) have developed the tumor, node, and metastases (TNM) staging system, which takes into account the degree of spread of the primary tumor, the extent of regional lymph node involvement, and the presence or absence of distant metastases (*Hassan, 2005*).

Thus, the choice of therapy options, including surgery, radiation therapy, and chemotherapy, each used alone or in combination with the other treatments, is based on the tumor stage. Hence, the accurate determination of tumor size, potential infiltration of adjacent structures, and mediastinal lymph node involvement, and the detection of distant metastases are of central importance (*Smythe, 2001*).

Normal PET and PET/CT anatomy

There are several sites of normal physiologic accumulation of Fluorodeoxyglucose (FDG). FDG accumulation is most intense in the cerebral cortex, basal ganglia, thalamus, and cerebellum, since the brain is exclusively dependent on glucose metabolism. The myocardium expresses insulin-sensitive glucose transporters, which facilitate the transport of glucose into muscle. Although the myocardium uses free fatty acids as its primary substrate, in the non fasting state the anti lipolytic effect of insulin reduces the delivery of free fatty acids, and the heart relies more on glycolytic metabolism. A recent meal often causes intense myocardial FDG uptake because of the associated elevated serum insulin levels. Fasting for 4–6 hours before FDG administration decreases the availability of both glucose and insulin in the circulation, which usually leads to decreased accumulation of FDG within the myocardium. Because FDG appears in the glomerular filtrate and, unlike glucose, is not reabsorbed in the tubules, intense FDG activity is seen in the intra renal collecting systems, ureters, and bladder. Less intense radiotracer activity is present in the liver, spleen, bone marrow, and renal cortex. At 1 hour after radiotracer injection, blood pool activity results in moderate background activity in the mediastinum, whereas lung activity is low.

Significant muscle uptake is observed in the skeletal muscles with exercise, in the breathing muscles with

hyperventilation, in the cervical muscles with tension, and in the laryngeal muscles with localization. Uptake in lymphatic tissues and salivary glands may also be seen as a normal variant. Uptake in the gastrointestinal tract is variable. Normal stomach, small intestine, and colon may demonstrate increased FDG uptake due to a combination of factors, including smooth muscle contraction and metabolically active mucosa (*Kostakoglu et al., 2003*) (*Fig 1 and 2*).

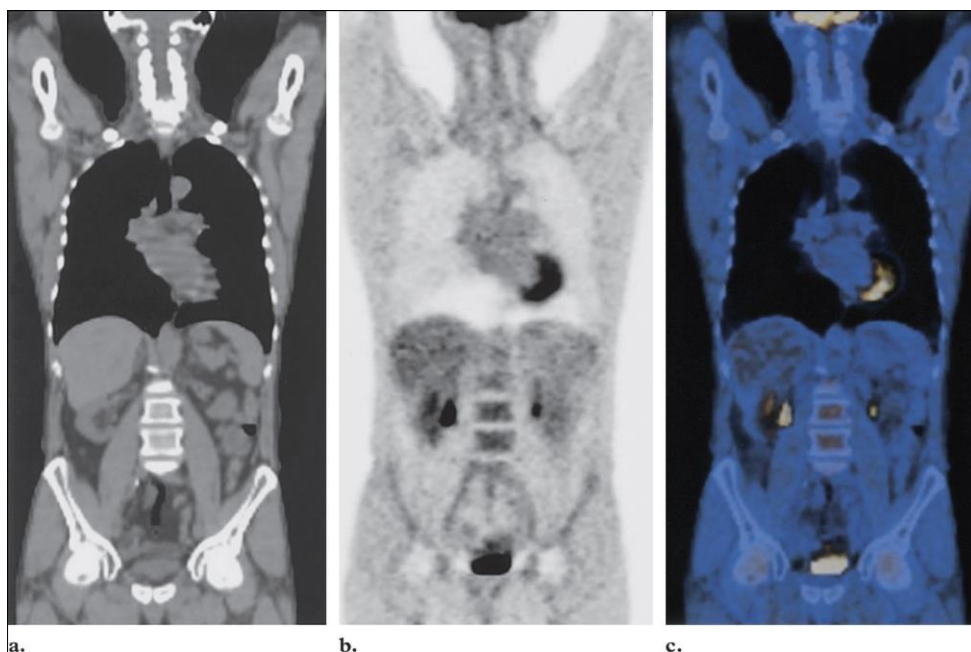


Figure 1. Normal distribution of FDG. Coronal CT (a), PET (b), and PET/CT fusion (c) images demonstrate the physiologic accumulation of FDG in the cerebral-cerebellar cortex at the base of the skull and in the myocardium, liver, kidneys, renal pelvis, bone marrow, and urinary bladder. Note also the minimal uptake in the mediastinum and bilaterally in the lower cervical and psoas muscles (*Quoted from Kostakoglu et al., 2003*).
